

The Halo Occupation Distribution of HI from 21cm Intensity Mapping at Moderate Redshifts

J. Stuart B. Wyithe¹, Michael J. I. Brown²

¹*School of Physics, University of Melbourne, Parkville, Victoria, Australia*

²*School of Physics, Monash University, Clayton, Victoria 3800, Australia*

Email: swyithe@unimelb.edu.au

5 November 2018

ABSTRACT

The spatial clustering properties of HI galaxies can be studied using the formalism of the halo occupation distribution (HOD). The resulting parameter constraints describe properties like gas richness versus environment. Unfortunately, clustering studies based on individual HI galaxies will be restricted to the local Universe for the foreseeable future, even with the deepest HI surveys. Here we discuss how clustering studies of the HI HOD could be extended to moderate redshift, through observations of fluctuations in the combined 21cm intensity of unresolved galaxies. In particular we make an analytic estimate for the clustering of HI in the HOD. Our joint goals are to estimate *i*) the amplitude of the signal, and *ii*) the sensitivity of telescopes like the Australian SKA Pathfinder to HOD parameters. We find that the power spectrum of redshifted 21cm intensity could be used to study the distribution of HI within dark matter halos at $z \gtrsim 0.5$ where individual galaxies cannot be detected. In addition to the HOD of HI, the amplitude of the 21cm power spectrum would also yield estimates of the cosmic HI content (Ω_{HI}) at epochs between the local Universe, and redshifts probed by damped Ly α absorbers.

Key words: cosmology: large scale structure, observations – galaxies: halos, statistics – radio lines: galaxies

1 INTRODUCTION

The cosmic star-formation rate has declined by more than an order of magnitude in the 8 billion years since $z \sim 1$ (Lilly et al. 1996, Madau et al. 1996). Why this decline has taken place, and what drove it are two of the most important unanswered questions in our current understanding of galaxy formation and evolution. In cold dark matter cosmologies, gas cools and collapses to form stars within gravitationally bound “halos” of dark matter. These galaxies can then grow via continued star formation or via mergers with other galaxies. As a result the decline in star formation at $z \lesssim 1$ is presumably accompanied by a decrease in the amount of cold gas within halos.

One of the issues that will need to be addressed in order to understand the evolution in star formation rate is the role of environment. As galaxies of a given baryonic mass can only reside within dark matter halos above a particular dark matter mass, galaxies are biased tracers of the overall dark matter distribution. The clustering of dark matter halos is a known function of their mass (e.g., Sheth, Mo & Tormen 2001), and consequently the large-scale clustering of galaxies provides an estimate of the typical halo mass

in which that galaxy population resides. On smaller scales, multiple galaxies can reside within a single ($\lesssim 1$ Mpc radius) dark matter halo, so that the number of galaxy pairs with small spatial separations is a strong function of the number of galaxies per halo. One can thus constrain the number of galaxies per halo as a function of halo mass by measuring both the small ($\lesssim 1$ Mpc) and large ($\gtrsim 1$ Mpc) scale clustering of galaxies (e.g. Peacock & Smith 2000, Zheng 2005). The clustering of galaxy samples selected to lie within different stages of galaxy formation based on their stellar and cold gas content therefore has the potential to play a central role in our understanding of the star formation history.

In recent years large galaxy redshift surveys such as SDSS and the 2dFGRS have enabled detailed studies of the clustering of more than 100,000 optically selected galaxies in the nearby universe. By using clustering to understand how galaxies populate dark matter halos, key insights may be obtained into how galaxies grow over cosmic time. The way in which stellar mass populates dark matter halos has been determined through studies of clustering for optically selected galaxy samples. A popular formalism for modeling clustering on small to large scales is termed the halo occupation distri-

bution (HOD; e.g. Peacock & Smith 2000; Seljak 2000; Scocimarro et al. 2001; Berlind & Weinberg 2002; Zheng 2004). The HOD includes contributions to galaxy clustering from pairs of galaxies in distinct halos which describes the clustering in the large scale limit, and from pairs of galaxies within a single halo which describes clustering in the small scale limit. The latter contribution requires a parametrisation to relate the number and spatial distribution of galaxies within a dark matter halo of a particular mass. It is by constraining this parameterisation that observed clustering can be used to understand how galaxies are distributed.

By comparison with the massive optical redshift surveys, the largest survey of HI selected galaxies contains only ~ 5000 sources, obtained as part of the HIPASS survey, a blind HI survey of the southern sky (Barnes et al. 2001). Meyer et al. (2007) have studied the clustering of these HI galaxies. Their analysis reached the conclusion of weak clustering of HI galaxies based on parametric estimates of correlation length, but did not study the clustering in terms of the host dark matter halo masses of the HIPASS sample. Wyithe, Brown, Zwaan & Meyer (2009) analysed the clustering properties of HI selected galaxies from the HIPASS survey using the formalism of the halo occupation distribution. They found that the real-space clustering amplitude for HIPASS galaxies is significant on scales below the virial radius associated with the halo mass required to reproduce the clustering amplitude on large scales, indicating that single halo pairs are contributing a 1-halo term. However the resulting parameter constraints show that satellite galaxies make up only $\sim 10\%$ of the HIPASS sample. HI satellite galaxies are therefore less significant in number and in terms of their contribution to clustering statistics than are satellites in optically selected galaxy redshift surveys.

These results from HOD modeling of HI galaxy clustering therefore quantify the extent to which environment governs the HI content of galaxies in the local Universe and confirms previous evidence that HI galaxies are relatively rare in overdense environments (Waugh et al. 2002; Cortes et al. 2008). Wyithe et al. (2009) found a minimum halo mass for HIPASS galaxies at the peak of the redshift distribution of $M \sim 10^{11} M_{\odot}$ (throughout this paper we refer to the halo mass as M and the HI mass as M_{HI}), and showed that less than 10% of baryons in HIPASS galaxies are in the form of HI. Their analysis also revealed that the fingers-of-god in the redshift space correlation function are sensitive to the typical halo mass in which satellite galaxies reside, and indicated that the HI rich satellites required to produce the measured 1-halo term must be preferentially in group rather than cluster mass halos.

As described above, the clustering of HI galaxies can be studied at $z = 0$ using HIPASS. However in the future with the advent of the Square Kilometer Array (SKA) and its pathfinders the volume and redshift range over which clustering of HI galaxies can be studied will greatly increase. On the other hand, these studies will still be limited to moderate redshifts of $z \lesssim 0.5$ owing to the sensitivity required for detection of even the most massive HI galaxies. For example, the Australian SKA pathfinder (ASKAP) will detect the most massive HI galaxies only out to $z \sim 0.7$ in the deepest integrations (Johnston et al. 2007). At higher redshifts, we argue that progress on the clustering of HI galaxies may be made by measurement of fluctuations in the com-

bined surface-brightness of unresolved HI galaxies (Wyithe & Loeb 2009; Chang et al. 2008; Wyithe 2008). A survey of 21cm intensity fluctuations at redshifts beyond those where individual galaxies can be detected would therefore measure the modulation of the cumulative 21cm emission from a large number of galaxies. The detectability of the 21 cm PS after reionization was discussed by Khandai et al. (2009). These authors used an N-body and simulation to predict the statistical signal of 21 cm fluctuations in the post-reionization IGM, and estimated its detectability. Khandai et al. (2009) find that a combination of these arrays offer good prospects for detecting the 21 cm PS over a range of redshifts in the post reionization era. Importantly, a statistical detection of 21 cm fluctuations due to discrete, unresolved clumps of neutral gas has already been made (Pen et al. 2008) through cross-correlation of the HIPASS (Barnes et al. 2001) 21 cm observations of the local universe with galaxies in the 6 degree field galaxy redshift survey (Jones et al. 2005). This detection represents an important step towards using 21 cm surface brightness fluctuations to probe the neutral gas distribution in the IGM.

The majority of the discussion in the literature concerning 21cm fluctuations in the low-redshift Universe has centered around their utility for cosmological constraint (Wyithe & Loeb 2009; Chang et al. 2008; Loeb & Wyithe 2009; Bharadwaj, Sethi & Saini 2009). In this paper we concentrate on the possibility of studying the distribution of HI within dark matter halos, on scales accessible to traditional configurations for radio interferometers (which do not include the very short baselines required to study the 21cm fluctuations in the large scale, linear regime). On these scales recent simulations suggest that the smoothed HI density field is highly biased owing to non-linear gravitational clustering (Bagla & Khandai 2009). Following from this prediction we discuss the possibility of studying the occupation of dark matter halos by HI at high redshift via 21cm intensity mapping. As a concrete example we consider the potential of ASKAP with respect to constraining the HI HOD. We concentrate on $z \sim 0.7$, as this is the redshift at which ASKAP no longer has the sensitivity to study individual galaxies. Our goal is not to provide a detailed method for extracting detailed HOD parameters from an observed power spectrum of redshifted 21cm fluctuations. This would require calibration against N-body simulations, which is premature at this time. Rather, we present an analytic model for the 21cm power spectrum in the HOD, and investigate which of its properties could be constrained by observations using a telescope like ASKAP

The paper is organised as follows. We begin by summarising the formalism for the HOD model, and introduce HOD modeling of 21cm intensity fluctuations in § 2. We discuss the potential sensitivity of ASKAP to these fluctuations in § 3. We then present our forecast constraints on HOD parameters in § 4 and describe estimates of the HI mass function in § 5. We summarise our findings in § 6. In our numerical examples, we adopt the standard set of cosmological parameters (Komatsu et al. 2009), with values of $\Omega_{\text{m}} = 0.24$, $\Omega_{\text{b}} = 0.04$ and $\Omega_{\text{Q}} = 0.76$ for the matter, baryon, and dark energy fractional density respectively, $h = 0.73$, for the dimensionless Hubble constant, and $\sigma_8 = 0.81$ for the variance of the linear density field within regions of radius $8h^{-1}\text{Mpc}$.

2 INTENSITY MAPPING AND THE HI HOD

We begin by reviewing the halo occupation distribution formalism for galaxies (e.g. Peacock & Smith 2000; Seljak 2000; Scoccimarro et al. 2001; Berlind & Weinberg 2002; Zheng 2004) which we describe only briefly, referring the reader to the above papers for details. The technique of surface brightness mapping will not allow resolution of individual galaxies, but rather the measurement of fluctuations in the surface brightness of unresolved galaxies. However we utilise a halo model formalism where galaxies are traced, rather than a form where the density field is a continuous function. This is because the HI is found in discrete galaxies, and treating individual galaxies allows us to explicitly calculate the HI mass weighted galaxy bias. The HOD model is constructed around the following simple assumptions. First, one assumes that there is either zero or one central galaxy that resides at the centre of each halo. Satellite galaxies are then assumed to follow the dark matter distribution within the halos. The mean number of satellites is typically assumed to follow a power-law function of halo mass, while the number of satellites within individual halos follows a Poisson (or some other) probability distribution. The two-point correlation function on a scale r can be decomposed into one-halo (ξ_{1h}) and two-halo (ξ_{2h}) terms

$$\xi(r) = [1 + \xi_{1h}(r)] + \xi_{2h}(r), \quad (1)$$

corresponding to contributions to the correlation function from galaxy pairs which reside in the same halo and in two different halos respectively (Zheng 2004).

The 2-halo term can be computed as the halo correlation function weighted by the distribution and occupation number of galaxies within each halo. The 2-halo term of the galaxy power spectrum (PS) is

$$P_{\text{gg}}^{2h}(k) = P_{\text{m}}(k) \left[\frac{1}{\bar{n}_{\text{g}}} \int_0^{M_{\text{max}}} dM \frac{dn}{dM} \langle N \rangle_M b(M) y_{\text{g}}(k, M) \right]^2, \quad (2)$$

where P_{m} is the mass PS and y_{g} is the normalised Fourier transform of the galaxy distribution, which is assumed to follow a Navarro, Frenk & White (1997; NFW) profile (see e.g. Seljak 2000; Zheng 2004). Here \bar{n}_{g} is the mean number density of galaxies. We assume the Sheth Tormen (1999) mass function dn/dM using parameters from Jenkins et al. (2001) throughout this paper. To compute the halo bias $b(M)$ we use the Sheth, Mo and Tormen (2001) fitting formula. The quantity M_{max} is taken to be the mass of a halo with separation $2r$. The 2-halo term for the correlation function follows from

$$\xi_{2h}(r) = \frac{1}{2\pi^2} \int_0^\infty P_{\text{gg}}^{2h}(k) k^2 \frac{\sin kr}{kr} dk. \quad (3)$$

In real space the 1-halo term can be computed using (Berlind & Weinberg 2002)

$$1 + \xi_{1h}(r) = \frac{1}{2\pi r^2 \bar{n}_{\text{g}}^2} \times \int_0^\infty dM \frac{dn}{dM} \frac{\langle N(N-1) \rangle_M}{2} \frac{1}{2R_{\text{vir}}(M)} F' \left(\frac{r}{2R_{\text{vir}}} \right), \quad (4)$$

where $\langle N(N-1) \rangle_M$ is the average number of galaxy pairs within halos of mass M . The distribution of multiple galaxies within a single halo is described by the function $F'(x)$, which is the differential probability that galaxy pairs are separated

by a dimensionless distance $x \equiv r/R_{\text{vir}}$. As is common in the literature, we assume that there is always a galaxy located at the center of the halo, and others are regarded as satellite galaxies. The contribution to F' is therefore divided into pairs of galaxies that do, and do not involve a central galaxy, and is computed assuming that satellite galaxies follow the number-density distribution of an NFW profile. With this assumption, the term in the integrand of equation (4) reads

$$\begin{aligned} & \langle N(N-1) \rangle_M F'(x) \\ &= \langle N-1 \rangle_M F'_{\text{cs}}(x) + \frac{\langle (N-1)(N-2) \rangle_M}{2} F'_{\text{ss}}(x). \end{aligned} \quad (5)$$

where $F'(x)$ is the pair-number-weighted average of the central-satellite pair distribution $F'_{\text{cs}}(x)$ and the satellite-satellite pair distribution $F'_{\text{ss}}(x)$ (see, e.g., Berlind & Weinberg 2002; Yang et al. 2003; Zheng 2004),

2.1 21cm intensity mapping of HI clustering

The HOD method of estimating and modeling the clustering of HI galaxies will not work at redshifts beyond $z \sim 0.7$, where even the most luminous galaxies will not be detectable in HI for the foreseeable future. Instead, observations of surface brightness fluctuations in 21cm intensity arising from the combined signal of a large number of unresolved galaxies could be used to measure the clustering of HI galaxies. Studies of 21cm surface brightness fluctuations over a large volume will be made possible by the widefield interferometers now coming on line, and will allow the HI properties of galaxies to be studied over a greater range of redshifts. Indeed, it has been argued that lack of identification of individual galaxies is an advantage when attempting to measure the clustering of the HI emission, since by not imposing a minimum threshold for detection, such a survey collects all the available signal. This point is discussed in Pen et al. (2008), where the technique is also demonstrated via measurement of the cross-correlation of galaxies with unresolved 21cm emission in the local Universe.

The situation is analogous to mapping of the three-dimensional distribution of cosmic hydrogen during the reionization era through the 21cm line (Furlanetto, Oh & Briggs 2007; Barkana & Loeb 2007). Several facilities are currently being constructed to perform this experiment (including MWA¹, LOFAR², PAPER³, 21CMA⁴) and more ambitious designs are being planned (SKA⁵). During the epoch of reionization, the PS of 21cm brightness fluctuations is shaped mainly by the topology of ionized regions. However the situation is expected to be simpler following reionization of the intergalactic medium (IGM; $z \lesssim 6$) – when only dense pockets of self-shielded hydrogen, such as damped Ly α absorbers (DLA) and Lyman-limit systems (LLS) survive (Wyithe & Loeb 2008; Chang et al. 2007; Pritchard & Loeb 2008). These DLA systems are thought to be the high redshift equivalents of HI rich galaxies in the local Universe (Zwaan et al. 2005b). We do not expect 21cm self absorption to impact the level of 21cm emission. This conclusion

¹ <http://www.haystack.mit.edu/ast/arrays/mwa/>

² <http://www.lofar.org/>

³ <http://astro.berkeley.edu/~dbacker/EoR/>

⁴ <http://web.phys.cmu.edu/~past/>

⁵ <http://www.skatelescope.org/>

is based on 21cm absorption studies towards damped Ly α systems at a range of redshifts between $z \sim 0$ and $z \sim 3.4$, which show optical depths to absorption of the back-ground quasar flux with values less than a few percent (Kanekar & Chengalur 2003; Curran et al. 2007). Moreover, damped Ly α systems have a spin temperature that is large relative to the temperature of the cosmic microwave background radiation, and will therefore have a level of emission that is independent of the kinetic gas temperature (e.g. Kanekar & Chengalur 2003). Thus the intensity of 21cm emission can be directly related to the column density of HI.

2.2 Modeling the power spectrum of 21cm fluctuations

As mentioned above, low spatial resolution observations could be used to detect surface brightness fluctuations in 21cm emission from the cumulative sum of HI galaxies, rather than from individual sources of emission. Here the PS is a more natural observable than the correlation function, since a radio interferometer records visibilities that directly sample the PS. In the linear regime the 21cm PS follows directly from the PS of fluctuations in mass $P_m(k)$ (Wyithe & Loeb 2009)

$$P_{\text{HI}}(k) \approx \mathcal{T}_{\text{b}}^2 x_{\text{HI}}^2 \langle b \rangle_M^2 P_m(k), \quad (6)$$

where $\mathcal{T}_{\text{b}} = 23.8 [(1+z)/10]^{\frac{1}{2}}$ mK is the brightness temperature contrast between the mean IGM and the CMB at redshift z , and $\langle b \rangle_M$ is the HI mass weighted halo bias. Note that we have used the subscript HI rather than the more usual $_{21}$ in order to reduce confusion with the subscripts for the 1-halo and 2-halo PS terms. The fraction of hydrogen that is neutral is described by the parameter $x_{\text{HI}} \equiv \Omega_{\text{HI}}/(0.76\Omega_{\text{b}})$. We assume $x_{\text{HI}} = 0.01$ (corresponding to $\Omega_{\text{HI}} \sim 3 \times 10^{-4}$, Zwaan et al. 2005a) throughout this paper. The resulting PS is plotted in the right panel of Figure 1 (dashed line). The constant \mathcal{T}_{b} hides the implicit assumptions that the 21cm emission from the galaxies is not self absorbed, and that the spin temperature is much larger than the temperature of the cosmic microwave background. On small scales a model is needed to relate HI mass to halo mass. To achieve this we modify the HOD formalism as outlined below.

2.2.1 HOD model for 21cm fluctuations

Since surface brightness fluctuations depend on the total HI mass within a halo rather than on number counts of individual galaxies, the number of galaxies, and the number of galaxy pairs per halo in the HOD formalism need to be weighted by the HI mass per galaxy. In analogy with the HOD formalism, we distribute this mass between central and satellite galaxies. We define $\langle M_{\text{HI},c} \rangle_M$ and $\langle M_{\text{HI},s} \rangle_M$ to be the mean HI mass of central galaxies and of the combined satellite galaxies within a halo of mass M respectively.

To compute the 2-halo PS, we replace $\langle N \rangle_M$ in equation (2) with the mean value of the total HI mass in a halo of mass M , i.e. $\langle M_{\text{HI}} \rangle_M = \langle M_{\text{HI},c} \rangle_M + \langle M_{\text{HI},s} \rangle_M$, yielding

$$P_{\text{HI,gg}}^{2\text{h}}(k) = \mathcal{T}_{\text{b}}^2 x_{\text{HI}}^2 P_m(k) \times \left[\frac{1}{\bar{\rho}_{\text{HI}}} \int_0^{M_{\text{max}}} dM \frac{dn}{dM} \langle M_{\text{HI}} \rangle_M b(M) y_{\text{g}}(k, M) \right]^2, \quad (7)$$

where, $\bar{\rho}_{\text{HI}}$ is the mean density of HI contributed by all galaxies in the IGM. The 2-halo term $\xi_{2\text{h,HI}}(r)$ follows from substitution into equation (3).

To compute the 1-halo term we again weight the number of galaxies by their HI mass. In difference from the calculation of the 1-halo term for galaxy clustering, the distribution of satellite masses will be important in addition to the number. This aspect of the HOD modeling will require simulation for a proper treatment (e.g. Bagla & Khandai 2009). However for the purposes of our analysis it is sufficient to assume that most of the satellite HI for a halo mass M is contained within satellites of similar mass (as would be the case for a steep power-law mass function with a lower cutoff for example). We therefore further define $\langle m_{\text{HI},s} \rangle_M$ to be the mean HI mass of satellite galaxies within a halo of mass M . The coefficients in equation (5) are then modified to yield

$$\langle (N-1) \langle m_{\text{HI},s} \rangle_M \times \langle M_{\text{HI},c} \rangle_M \rangle = \langle M_{\text{HI},c} \rangle_M \langle M_{\text{HI},s} \rangle_M \quad (8)$$

and

$$\frac{\langle (N-1) \langle m_{\text{HI},s} \rangle_M \times (N-2) \langle m_{\text{HI},s} \rangle_M \rangle}{2} = \frac{\langle M_{\text{HI},s} \rangle_M^2}{2} \quad (9)$$

respectively. To calculate this second term we have noted that for a Poisson distribution of galaxies $\langle (N-1)(N-2) \rangle_M = \langle (N-1) \rangle_M^2$, and have assumed that $\langle M_s \rangle_M = \langle (N-1) \rangle_M \times \langle m_s \rangle_M$. The modified expression for the 1-halo term therefore becomes⁶

$$\mathcal{T}_{\text{b}}^2 x_{\text{HI}}^2 + \xi_{1\text{h,HI}}(r) = \frac{\mathcal{T}_{\text{b}}^2 x_{\text{HI}}^2}{2\pi r^2 \bar{\rho}_{\text{HI}}^2} \int_0^\infty \frac{dn}{dM} \left[\langle M_{\text{HI},c} \rangle_M \langle M_{\text{HI},s} \rangle_M F'_{\text{cs}} \left(\frac{r}{2R_{\text{vir}}} \right) + \frac{\langle M_{\text{HI},s} \rangle_M^2}{2} F'_{\text{ss}} \left(\frac{r}{2R_{\text{vir}}} \right) \right] \frac{1}{R_{\text{vir}}(M)} dM. \quad (10)$$

The correlation function follows from $\xi_{\text{HI}}(r) = [\mathcal{T}_{\text{b}}^2 x_{\text{HI}}^2 + \xi_{1\text{h,HI}}(r)] + \xi_{2\text{h,HI}}(r)$.

In order to evaluate this expression the HI mass occupation of a halo of mass M must be parameterised, and is obviously quite uncertain. For illustration, we choose the following polynomial form, with a minimum halo mass (M_{min}) and characteristic scale (M_1) where satellites contribute HI mass that is comparable to the central galaxy,

$$\langle M_{\text{HI},c} \rangle_M \propto M^{\gamma_c} \quad \text{if } M > M_{\text{min}} \\ = 0 \quad \text{otherwise.} \quad (11)$$

and

$$\langle M_{\text{HI},s} \rangle_M = M_{\text{HI},c} \left(\frac{M}{M_1} \right)^{\gamma_s} \quad \text{if } M > M_{\text{min}} \\ = 0 \quad \text{otherwise.} \quad (12)$$

The average HI mass within a halo of mass $M > M_{\text{min}}$ is therefore

$$\langle M_{\text{HI}} \rangle_M = \langle M_{\text{HI},c} \rangle_M + \langle M_{\text{HI},s} \rangle_M \propto M^{\gamma_c} \left[1 + \left(\frac{M}{M_1} \right)^{\gamma_s} \right] \quad (13)$$

Note that the constant of proportionality in equations (11) and (13) is not specified but cancels with the same factor

⁶ Note that the correlation function has dimensions of mK, and therefore does not have the usual interpretation of probability above random for finding a galaxy pair of separation r .

in ρ_{HI} in equations (7) and (10). From experience of the galaxy HOD there will be degeneracy between the parameters M_1 and γ_s . We therefore make the simplification of setting $\gamma_c = \gamma_s \equiv \gamma$ in our parameterisation for the remainder of this paper. The left panel of Figure 1 shows the real-space correlation function at $z = 0.7$ for an HOD model with parameters $\gamma = 0.5$, $M_{\text{min}} = 10^{11}M_{\odot}$ and $M_1 = 10^{13}M_{\odot}$. This model serves as our fiducial case throughout this paper, and is motivated by the parameters derived from estimates for HIPASS galaxies (Wyithe et al. 2009). In particular we note the value of $\gamma = 0.5$ which is smaller than unity. This value encapsulates the assumption that smaller halos have more HI, and agrees with the conventional wisdom that galaxy clusters are HI poor. In the local Universe $\gamma \sim 0.5$ is found to describe the relation between HI and dynamical masses of HIPASS galaxies (Wyithe et al. 2009). Aside from this motivation the fiducial model is otherwise arbitrary.

2.2.2 Redshift space modeling of the 21cm power spectrum

Since a radio interferometer directly measures the 3 dimensional distribution of 21cm intensity it is more powerful to work in redshift space, where line-of-sight infall (Kaiser 1987) can be used to break the degeneracy between neutral fraction and galaxy bias (Wyithe 2008). In addition to gravitational infall the shape of the redshift space PS will be complicated by peculiar motions of galaxies within groups or clusters, which produce the so-called fingers-of-god in the redshift space correlation function. In the case of 21cm fluctuations, the internal velocities of HI in galaxies will also contribute to the fingers-of-god. In this paper we use the combination of the real-space HOD 21cm PS

$$P_{\text{R,HI}}(k) = 4\pi \int dr \xi_{\text{HI}}(r) \frac{\sin kr}{kr} r^2 dr, \quad (14)$$

and the dispersion model to estimate the redshift space PS including these effects. The dispersion model is written

$$P_{z,\text{HI}}(k_{\text{perp}}, k_{\text{los}}) = P_{\text{R,HI}}(k) (1 + \beta\mu^2)^2 (1 + k^2 \sigma_k^2 \mu^2 / 2)^{-1} \quad (15)$$

where μ is the cosine of the angle between the line-of-sight and the unit-vector corresponding to the direction of a particular mode, $k_{\text{perp}} = k\mu$, $k_{\text{los}} = k\sqrt{1 - \mu^2}$, $\beta = \Omega_{\text{m}}^{0.6} / \langle b \rangle_{\text{M}}$ and $\langle b \rangle_{\text{M}}$ is the average HI mass weighted halo bias. The quantity σ_k is a constant which describes a ‘‘typical’’ velocity dispersion for galaxies and parametrises the prominence of the fingers-of-god. Simulations indicate a value of $\sigma_k \sim 650/(1+z)\text{km s}^{-1}$ (Lahav & Suto 2004). We note that the redshift space PS could have been generated through a 2-d Fourier transform of the redshift space correlation function computed within the HOD model using the formalism described in Tinker (2007), allowing additional constraints on HOD parameters to be placed based on the prominence of the fingers-of-god as in Wyithe et al. (2009). In particular the assumption of $\gamma < 1$ as well as the potential lack of HI in clusters would lead to reduced prominence of the fingers of god. However in the absence of current data we have taken the simpler approach of parameterising the fingers-of-god using σ_k .

The left panel of Figure 2 shows the resulting redshift space PS for the fiducial model. The large scale motions induced by infall into overdense regions can be seen as an

extension of the PS along the line-of-sight at small k , while the fingers of god are manifest as a compression at large k . The right panel of Figure 1 shows the corresponding spherically averaged redshift space PS (solid line)

$$P_{z,\text{HI}}^{\text{sph}}(k) = \int P_{z,\text{HI}}(k_{\text{perp}}, k_{\text{los}}) dk_{\text{perp}} dk_{\text{los}}. \quad (16)$$

For comparison, the dotted lines in the right hand panel of Figure 2 show the 1-halo and 2-halo contributions to the spherically averaged redshift space PS.

The spherically averaged redshift space PS can be compared with the linear real-space 21cm PS estimated based on the neutral fraction $x_{\text{HI}} = 0.01$ and the linear mass PS (dashed line, equation 6). On large (linear) scales the spherically averaged PS is larger in redshift space than in real space. This is analogous to the excess power seen in redshift space clustering of galaxy surveys (Kaiser 1987), and is due to an increase in the 21cm optical depth owing to velocity compression (Barkana & Loeb 2005) towards high density regions. On small scales there is excess power above the linear theory expectation owing to the inclusion of the non-linear 1-halo term. The 21cm PS shows a steepening at large k owing to the mass weighting in the 1-halo term. This steepening is also seen in the simulations of Bagla & Khandai (2009).

2.2.3 variation of the 21cm PS with HOD parameters

Figure 3 illustrates the sensitivity of the clustering and the 21cm PS to variations in the HOD parameters. The solid lines repeat the fiducial model from Figure 1. For comparison, the dotted, dashed and dot-dashed lines show variations on this model, with $\gamma = 0.4$, $M_{\text{min}} = 10^{10}M_{\odot}$ and $M_1 = 10^{12}M_{\odot}$ respectively (with the remaining parameters set to their fiducial values in each case). On the largest scales the clustering amplitude is most sensitive to M_{min} (dashed lines), which enables the typical host halo mass of HI to be measured from the PS amplitude (Wyithe 2008). Lowering the value of M_{min} (while keeping M_1 fixed) implies a smaller fraction of HI in satellites, and hence a relative decrease of power on small scales. A smaller value of γ also leads to a relative decrease of power on small scales because the flatter power-law preferentially places mass in the more common low mass halos (with $M < M_1$), and so lowers the fraction of HI in satellites (dotted lines). Conversely, a smaller value of M_1 leads to a larger fraction of HI in satellite systems, and hence an increase of small scale power (dot-dashed lines).

The variation in shape and amplitude of the 21cm PS implies that parameter values for a particular HOD model could be constrained if the PS were measured with sufficient signal-to-noise. In the remainder of this paper we therefore first discuss the sensitivity of a radio interferometer to the 21cm PS, and then estimate the corresponding constraints on the 5 parameters in our HOD model that could be placed using observations of 21cm intensity fluctuations.

3 SENSITIVITY TO THE 21CM PS

In this paper we estimate the ability of a telescope like ASKAP to measure the clustering of 21cm intensity fluctuations, and hence to estimate HOD parameters, and the

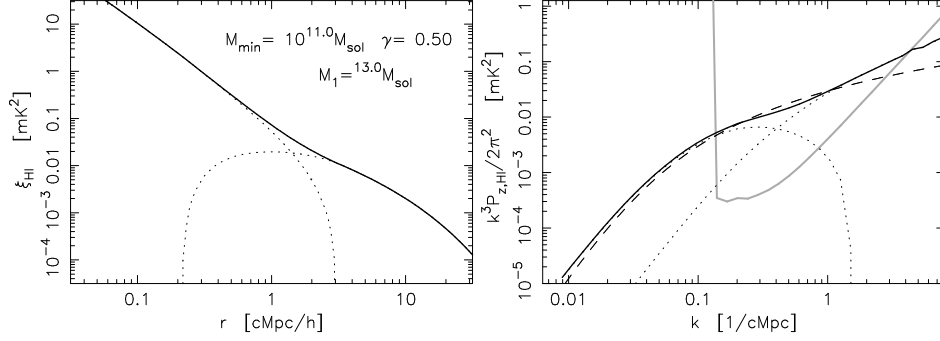


Figure 1. An example of the correlation function and PS of intensity fluctuations for a hypothetical HOD model at $z = 0.7$. *Left-hand panel:* the model correlation function. *Right-hand panel:* The corresponding spherically averaged redshift space PS (solid line). In each case the 1-halo and 2-halo terms are plotted as dotted curves. For comparison we plot the spherically averaged sensitivity within pixels of width $\Delta k = k/10$ for an a radio interferometer resembling the design of ASKAP (thick gray line). We also show the real-space 21cm PS assuming a linear mass-density PS (dashed line). For calculation of observational noise an integration of 3000 hours was assumed, with a multiple primary beam total field of view corresponding to $30(1+z)^2$ square degrees (see text for details). The cutoff at large scales is due to foreground removal within a finite frequency band-pass.

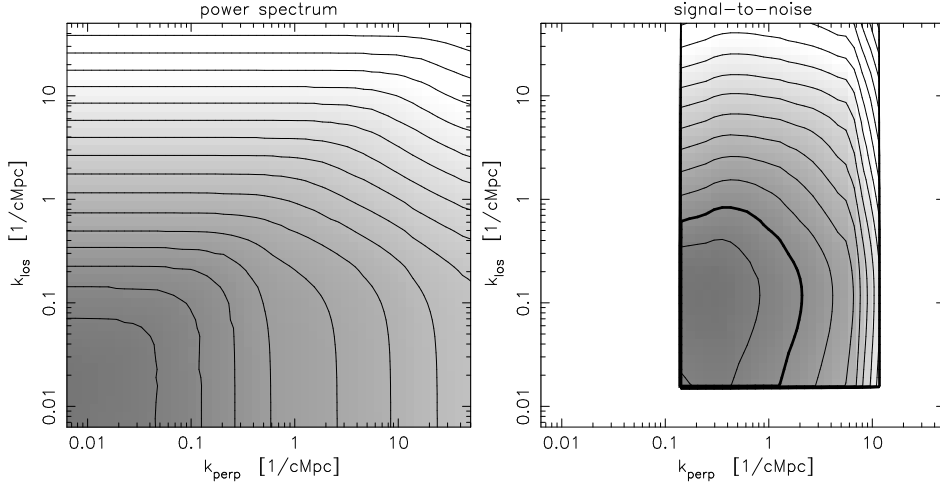


Figure 2. The redshift space PS of intensity fluctuations corresponding to the example in Figure 1. *Left-hand panel:* The redshift-space PS assuming a dispersion model with $\sigma_k = 650/(1+z)\text{km s}^{-1}$. *Right-hand panel:* Contours of the signal-to-noise (separated by factors of $\sqrt{10}$) within pixels of width $\Delta k = k/10$. The thick contour corresponds to a signal-to-noise per pixel of unity. For calculation of observational noise an integration of 3000 hours was assumed, with a multiple primary beam total field of view corresponding to $30(1+z)^2$ square degrees (see text for details). The cutoffs at large and small scales perpendicular to the line-of-sight are due to the lack of short and long baselines respectively. The cutoff at large scales along the line-of-sight is due to foreground removal within a finite band-pass.

total HI content of the Universe. The latter quantity, which is not available from the clustering of resolved galaxies, could be used to bridge the gap in measurements of Ω_{HI} (the cosmic density of HI relative to the critical density) between the local Universe where this quantity can be determined from integration of the HI mass function, and $z \gtrsim 2$ where it is measured from the column density through counting of damped Ly α absorbers.

To compute the sensitivity $\Delta P_{\text{HI}}(k_{\text{perp}}, k_{\text{los}})$ of a radio-interferometer to the 21cm PS, we follow the procedure outlined by McQuinn et al. (2006) and Bowman, Morales & Hewitt (2007) [see also Wyithe, Loeb & Geil (2008)]. The important issues are discussed below, but the reader is referred to these papers for further details. The uncertainty comprises components due to the thermal noise, and due to sample variance within the finite volume of the ob-

servations. We also include a Poisson component due to the finite sampling of each mode (Wyithe 2008), since the post-reionization 21cm PS is generated by discrete clumps rather than a diffuse IGM. We consider a telescope based on ASKAP. This telescope is assumed to have 36 dish antenna with a density distributed as $\rho(r) \propto r^{-2}$ within a diameter of 2km. The antennae are each 12m in diameter, and being dishes are assumed to have physical and effective collecting areas that are equal. We assume that foregrounds can be removed over 80MHz bins, within a band-pass of 300MHz [based on removal within 1/4 of the available bandpass (McQuinn et al. 2006)]. Foreground removal therefore imposes a minimum on the wave-number accessible of $k \sim 0.02[(1+z)/1.5]^{-1}\text{Mpc}^{-1}$, although access to the large scale modes is actually limited by the number of short baselines available. An important ingredient is the an-

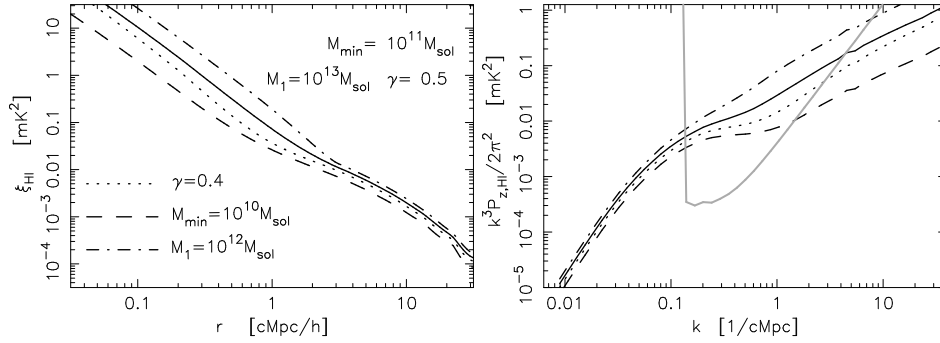


Figure 3. Examples of correlation functions (*left panel*) and spherically averaged redshift space PS (*right panel*) of intensity fluctuations for different HOD models at $z = 0.7$. The solid lines repeat the fiducial model from Figure 1 (parameters listed in the top-right corner of the left panel). For comparison, the dotted, dashed and dot-dashed lines show variations on this model, with $\gamma = 0.4$, $M_{\min} = 10^{10} M_{\odot}$ and $M_1 = 10^{12} M_{\odot}$ respectively (with the remaining parameters set to their fiducial values in each case). For comparison with the PS, we also plot the spherically averaged sensitivity within pixels of width $\Delta k = k/10$ for an a radio interferometer resembling the design of ASKAP (*right panel*, thick grey line).

gular dependence of the number of modes accessible to the array (McQuinn et al. 2006). ASKAP is designed to have multiple primary beams facilitated by a focal plane phased array. We assume 30 fields are observed simultaneously for 3000 hr each, yielding $\sim 30(1+z)^2$ square degrees [where the factor of $(1+z)^2$ originates from the frequency dependence of the primary beam]. The signal-to-noise for observation of the PS in the left panel of Figure 2 is shown in the right panel of Figure 2. A telescope like ASKAP would be most sensitive to modes of $k_{\text{perp}} \sim 0.1 - 1 \text{Mpc}^{-1}$ and $k_{\text{los}} \sim 0.03 - 0.3 \text{Mpc}^{-1}$. The spherically averaged signal-to-noise (within bins of $\Delta k = k/10$) is shown in the right panels of Figures 1 and 3 (grey curves). Comparison of the noise curve with the variability of the PS amplitude and shape among different HOD models for the 21cm PS (Figure 3) indicates that a telescope like ASKAP would be sufficiently sensitive to generate constraints on the HOD. Moreover, the spatial scale on which the array would be most sensitive corresponds to wave-numbers where we expect 1-halo and 2-halo contributions to be comparable, indicating that such observations may constrain HOD model parameters. This statement is quantified in the next section.

4 CONSTRAINTS ON HOD PARAMETERS FROM 21CM INTENSITY MAPPING

Based on our estimate of the sensitivity to the 21cm PS we forecast the ability of ASKAP to constrain the HI HOD. To begin, we assume the fiducial model $P_{z,\text{HI}}^{\text{true}}(k_{\text{perp}}, k_{\text{los}})$, as shown in Figure 2, and estimate the accuracy with which the parameters could be inferred. Our HOD model for the 21cm PS has five parameters, M_{\min} , M_1 , γ , x_{HI} and σ_k . For combinations of these parameters (M_{\min} , M_1 , γ , x_{HI} , σ_k) that differ from the fiducial case ($10^{11} M_{\odot}$, $10^{13} M_{\odot}$, 0.5, 0.01, $650/(1+z) \text{km/s}$), we compute a trial model for the real space correlation function. We then use this to calculate the chi-squared of the difference between the fiducial and the

trial models

$$\chi^2 = \sum_{k_{\text{perp}}} \sum_{k_{\text{los}}} \left(\frac{P_{z,\text{HI}}^{\text{true}} - P_{z,\text{HI}}(k_{\text{perp}}, k_{\text{los}} | M_{\min}, M_1, \gamma, x_{\text{HI}}, \sigma_k, \sigma_8)}{\Delta P_{z,\text{HI}}(k_{\text{perp}}, k_{\text{los}})} \right)^2, \quad (17)$$

and hence find the likelihood

$$\mathcal{L}(M_{\min}, M_1, \gamma, x_{\text{HI}}, \sigma_k) = \int d\sigma_8 \frac{dp}{d\sigma_8} \exp\left(-\frac{\chi^2}{2}\right). \quad (18)$$

The uncertainty introduced through imperfect knowledge of the PS amplitude (which is proportional to the normalization of the primordial PS, σ_8) is degenerate with x_{HI} (Wyithe 2008). For this reason the uncertainty in σ_8 has been explicitly included in equation (18). We assume a Gaussian distribution $dp/d\sigma_8$ for σ_8 with $\sigma_8 = 0.81 \pm 0.03$ (Kotatsu et al. 2009).

Figure 4 shows an example of forecast constraints on HOD model parameters for a telescope like ASKAP, assuming a 3000hr integration of a single pointing [$\sim 30(1+z)^2$ square degrees] centered on $z = 0.7$. Results are presented in the upper panels of Figures 4 which shows contours of the likelihood in 2-d projections of this 5-parameter space. Here prior probabilities on $\log x_{\text{HI}}$, $\log M_{\min}$, $\log M_1$, γ and σ_k are assumed to be constant. The contours are placed at 60%, 30% and 10% of the peak likelihood. The lower panels show the marginalised likelihoods on the individual parameters x_{HI} , M_{\min} , M_1 and γ .

A deep integration of a single pointing for a telescope like ASKAP would place some constraints on the minimum mass (the projected uncertainty on M_{\min} is ~ 0.5 dex), and measure the relationship between HI and halo mass (a $\sim 20\%$ constraint on γ). In addition to these constraints on the halo occupation distribution of HI, observations of the 21cm PS would also provide a measurement of the global neutral fraction (or equivalently Ω_{HI}), which would be constrained with a relative uncertainty of 20% at $z \sim 0.7$. This indicates that 21cm intensity fluctuations could be used to measure the evolution of Ω_{HI} from $z \sim 1$ to the present day, even though ASKAP will not detect individual galaxies at $z \gtrsim 0.7$ (Johnston et al. 2007). Measurement of Ω_{HI} based on the redshift space PS would be complementary to the detection of individual rare peaks, which could facilitating

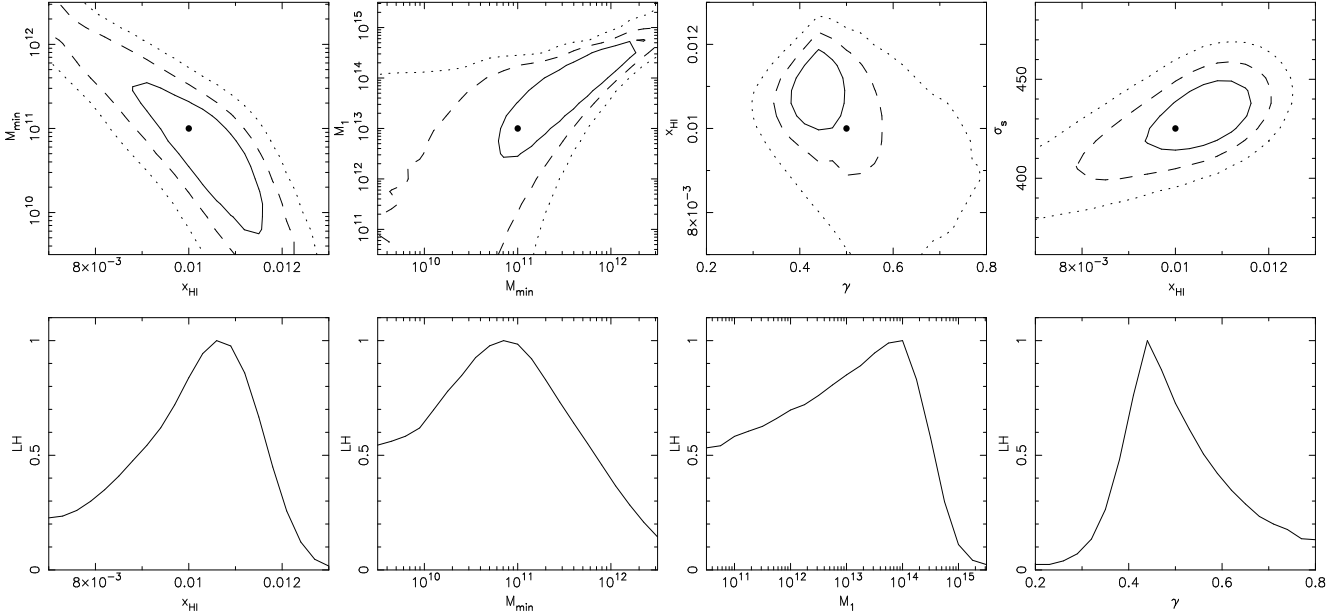


Figure 4. Example of forecast constraints on HOD model parameters from 21cm intensity fluctuations, assuming a 3000hr integration of a $30(1+z)^2$ square degree field with an array based on the ASKAP design centered on $z = 0.7$ (further details in the text). The *upper panels* show contours of the likelihood in 2-d projections of the 5-parameter space used for the HOD modeling of 21cm intensity fluctuations, while the *lower panels* show the marginalised likelihoods on individual parameters. Here prior probabilities on γ , $\log x_{\text{HI}}$, $\log M_{\text{min}}$ and $\log M_1$ are assumed to be constant. The contours are placed at 60%, 30% and 10% of the peak likelihood. The position of the dot indicates the peak likelihood in the 5-dimensional parameter space (i.e. the input model).

a direct estimate of the cosmic HI mass density (Bagla & Khandaï 2009).

5 HI CONTENT AND THE HI MASS FUNCTION

The combination of measurements for x_{HI} and the HOD parameters γ , M_{min} and M_1 indicates that the HI mass function (summing both central and satellite galaxies) could be approximated from the HOD using

$$\frac{dn}{dM_{\text{HI}}} = \frac{dn}{dM} \frac{dM}{dM_{\text{HI}}}. \quad (19)$$

where $M_{\text{HI}} = CM^\gamma(1 + (M/M_1)^\gamma)$ and the constant C is evaluated from

$$C = x_{\text{HI}} \frac{0.76(\Omega_b/\Omega_M)\rho_m}{\int_{M_{\text{min}}}^{\infty} M^\gamma \left(1 + \left(\frac{M}{M_1}\right)^\gamma\right) \frac{dn}{dM} dM}. \quad (20)$$

The left panel of Figure 5 shows the mass function for the fiducial model in Figure 1 (thick grey curve) as well as ten HI mass functions computed assuming parameters drawn at random from the joint probability distribution [$\propto M_{\text{min}}^{-1} M_1^{-1} x_{\text{HI}}^{-1} \mathcal{L}(M_{\text{min}}, M_1, \gamma, x_{\text{HI}}, \sigma_8)$], projections of which are shown in Figure 4. While the values over which the HI mass range extends in these realisations shows some variability, the possibility of constraints on γ and x_{HI} implied by Figure 4 mean that the overall shape of the HI mass function could be quite well constrained by observation of a redshifted 21cm PS. In the central panel of Figure 5 we show the corresponding the HI mass functions for central galaxies [obtained by instead substituting $M_{\text{HI}} = CM^\gamma$]. In this case the range of realisations is much larger, which can

be traced to the degeneracy between M_{min} and M_1 seen in Figure 4.

In addition to the HI mass function, it would also be possible to constrain the fraction of hydrogen within galaxies that is in atomic form. This number is given by

$$f_{\text{HI}} = \frac{x_{\text{HI}}}{F_{\text{col}}(M_{\text{min}})}, \quad (21)$$

where $F_{\text{col}}(M_{\text{min}})$ is the fraction of dark-matter that is collapsed in halos more massive than M_{min} . From the upper left panel of Figure 4 we see that there is a degeneracy between x_{HI} and M_{min} . Larger neutral fractions correspond to lower values of M_{min} and hence larger collapsed fractions. As a result the ratio f_{HI} would be very well constrained, as shown by the likelihood distribution in the right hand panel of Figure 5 (which is based on the distributions in the left panel of Figure 5). The evolution of f , which can also be measured locally from clustering with a value of $f_{\text{HI}} = 10^{-1.4 \pm 0.4}$ (Wyithe, Brown, Zwaan & Meyer 2009) will provide an important ingredient for studies of the role of HI in star formation.

6 SUMMARY

Due to the faintness of HI emission from individual galaxies, even deep HI surveys will be limited to samples at relatively low redshift ($z \lesssim 0.7$) for the next decade. However these surveys will be able to detect fluctuations in 21cm intensity produced by the ensemble of galaxies out to higher redshifts, using observational techniques that are analogous to those being discussed with respect to the reionization epoch at $z \gtrsim 6$ (e.g. Furlanetto, Oh & Briggs 2006). As

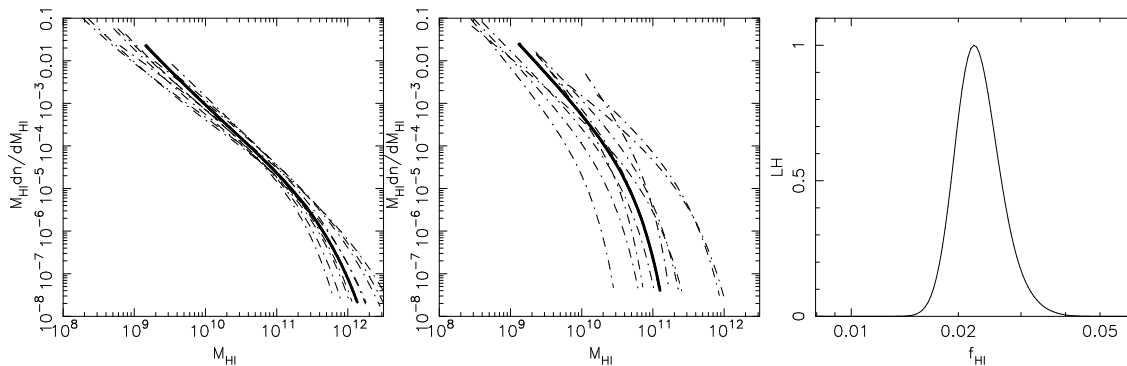


Figure 5. Examples of the range for the total halo (left) and central galaxy (central panel) HI mass functions. In addition to the fiducial case (thick lines, corresponding to the model in Figure 1), ten HI mass functions are shown in each case with parameters drawn from the probability distribution for HOD parameters in Figure 4 (dot-dashed lines). In the right panel we show forecast for corresponding constraints on f_{HI} . A 3000hr integration of a $30(1+z)^2$ square degree field with an array based on the ASKAP design centered on $z = 0.7$ (corresponding to Figure 4) was assumed. The prior probability on $\log f_{\text{HI}}$ was assumed to be constant.

a result, studies of HI galaxy clustering could be extended to redshifts beyond those where individual HI galaxies can be identified through the use of 21cm intensity fluctuations. To investigate this possibility we have described an approximate model for the power spectrum of 21cm fluctuations, which is based on the halo occupation distribution formalism for galaxy clustering. Our goal for this paper has been to use this model to estimate the expected amplitude and features of the 21 cm power-spectrum, rather than to present a detailed method for extracting the halo occupation of HI from an observed power-spectrum. This latter goal would require numerical simulations (e.g. Bagla & Khandai 2009).

To frame our discussion we have made forecasts for ASKAP, specifically with respect to the use of the 21cm power spectrum as a probe of the occupation of HI in dark matter halos. We have chosen $z = 0.7$ for our estimates, which is the redshift at which individual galaxies are no longer detectable with ASKAP in deep integrations. We have shown that a telescope based on the design of ASKAP will have sufficient sensitivity to yield estimates of the HI halo occupation. Because 21cm intensity fluctuations combine the integrated HI from all galaxies (not just those detected as individual sources), the clustering amplitude is proportional to the total HI content of the Universe. We find that an array with the specifications of ASKAP could yield estimates of the global HI density which have a relative accuracy of $\sim 20\%$. Clustering measurements in 21cm surface brightness could therefore be used to make measurements of the global HI content in the currently unexplored redshift range between the local Universe, and surveys for damped Ly α absorbers in the higher redshift Universe.

The cosmic star-formation rate has declined by more than an order of magnitude in the past 8 billion years (Lilly et al. 1996, Madau et al. 1996). Optical studies paint a somewhat passive picture of galaxy formation, with the stellar mass density of galaxies gradually increasing and an increasing fraction of stellar mass ending up within red galaxies that have negligible star-formation (e.g., Brown et al. 2008). On the other hand, the combination of direct HI observations at low redshift (Zwaan et al. 2005; Lah et al 2007) and damped Ly α absorbers in the spectra of high-redshift QSOs (Prochaska et al. 2005) show that the neutral gas den-

sity has remained remarkably constant over the age of the universe. The evolutionary and environmental relationships between the neutral gas which provides the fuel for star formation and the stars that form are central to understanding these and related issues. The study of the halo occupation distribution of HI based on 21cm fluctuations has the potential to allow these studies to be made at redshifts beyond those where individual galaxies can be observed in HI with either existing or future radio telescopes.

Acknowledgments. The research was supported by the Australian Research Council (JSBW).

REFERENCES

- Bagla, J. S., & Khandai, N. 2009, arXiv:0908.3796
 Barkana, R. & Loeb, A., 2007, Reports of Progress in Physics 70, 627.
 Barnes, D. G., et al. 2001, MNRAS, 322, 486
 Berlind, A. A., & Weinberg, D. H. 2002, ApJ, 575, 587
 Bharadwaj, S., Sethi, S. K., & Saini, T. D. 2009, Phys. Rev. D, 79, 083538
 Bowman, J.D., Morales, M.F. & Hewitt, J.N., 2007, Astrophys. J., 661, 1
 Brown, M. J. I., et al. 2008, ApJ, 682, 937
 Cortese, L., et al. 2008, MNRAS, 383, 1519
 de Blok, W. J. G., Zwaan, M. A., Dijkstra, M., Briggs, F. H., & Freeman, K. C. 2002, Astron. Astrophys., 382, 43
 Chang, T.-C., Pen, U.-L., Peterson, J.B. & McDonald, P., 2007, ArXiv-prints, 709, arXiv:0709.3672
 Curran, S.J., Tzanavaris, P., Pihlström, Y.M. & Webb, J.K., 2007, Mon. Not. R. Astron. Soc., 382, 1331
 Furlanetto, S. R., Oh, S. P. & Briggs, F. H., 2006, Phys. Rep. 433, 181.
 Hatton, S., & Cole, S. 1998, MNRAS, 296, 10
 Jenkins, A., Frenk, C. S., White, S. D. M., Colberg, J. M., Cole, S., Evrard, A. E., Couchman, H. M. P., & Yoshida, N. 2001, MNRAS, 321, 372
 Jones, D. H., Saunders, W., Read, M., & Colless, M. 2005, Publications of the Astronomical Society of Australia, 22, 277
 Kaiser, N., 1987, Mon. Not. R. Astron. Soc, 227, 1

- Kanekar, N., & Chengalur, J. N. 2003, *Astron. Astrophys.*, 399, 857
- Khandai, N., Datta, K. K., & Bagla, J. S. 2009, arXiv:0908.3857
- Komatsu, E., et al. 2009, *ApJS*, 180, 330
- Lah, P., et al. 2007, *MNRAS*, 376, 1357
- Ofer Lahav and Yasushi Suto, *Living Rev. Relativity*, 7, (2004), 8. [Online Article]: cited [2009], <http://www.livingreviews.org/lrr-2004-8>
- Lilly, S. J., Le Fevre, O., Hammer, F., & Crampton, D. 1996, *ApJL*, 460, L1
- Loeb, A., & Wyithe, J. S. B. 2008, *Physical Review Letters*, 100, 161301
- Madau, P., Ferguson, H. C., Dickinson, M. E., Giavalisco, M., Steidel, C. C., & Fruchter, A. 1996, *MNRAS*, 283, 1388
- McQuinn, M., Zahn, O., Zaldarriaga, M., Hernquist, L. & Furlanetto, S.R., 2006, *Astrophys. J.* 653, 815
- Meyer, M. J., Zwaan, M. A., Webster, R. L., Brown, M. J. I., & Staveley-Smith, L. 2007, *ApJ*, 654, 702
- Navarro, J. F., Frenk, C. S., & White, S. D. M. 1997, *ApJ*, 490, 493
- Peacock, J. A., & Smith, R. E. 2000, *MNRAS*, 318, 1144
- Pen, U.-L., Staveley-Smith, L., Peterson, J. & Chang, T.-C., 2008, ArXiv e-prints, 802, arXiv:0802.3239
- Pritchard, J.R. & Loeb, A., 2008, ArXiv e-prints, 802, arXiv:0802.2102
- Prochaska, J. X., Herbert-Fort, S., & Wolfe, A. M. 2005, *ApJ*, 635, 123
- Soccimarro, R., Sheth, R. K., Hui, L., & Jain, B. 2001, *ApJ*, 546, 20
- Seljak, U. 2000, *MNRAS*, 318, 203
- Sheth, R. K., & Tormen, G. 2002, *MNRAS*, 329, 61
- Sheth, R.K., Mo, H.J. & Tormen, G., 2001, *Mon. Not. R. Astron. Soc.*, 323, 1
- Tinker, J. L. 2007, *MNRAS*, 374, 477
- Waugh, M., et al. 2002, *MNRAS*, 337, 641
- Wyithe, J. S. B. 2008, *MNRAS*, 388, 1889
- Wyithe, J.S.B. & Loeb, A., 2008 *Mon. Not. R. Astr. Soc.*, 383, 606
- Wyithe, S., & Loeb, A. 2009, arXiv:0808.2323
- Wyithe, J.S.B., Loeb, A. & Geil, P.M., 2008, *Mon. Not. R. Astr. Soc.*, 383, 1195
- Wyithe, S., Brown, M. J. I., Zwaan, M. A., & Meyer, M. J. 2009, arXiv:0908.2854
- Zwaan, M. A., Meyer, M. J., Staveley-Smith, L., & Webster, R. L. 2005a, *MNRAS*, 359, L30
- Zwaan, M. A., van der Hulst, J. M., Briggs, F. H., Verheijen, M. A. W., & Ryan-Weber, E. V. 2005b, *MNRAS*, 364, 1467
- Zheng, Z. 2004, *ApJ*, 610, 61